HHS Public Access

Author manuscript

Int J Radiat Oncol Biol Phys. Author manuscript; available in PMC 2022 June 01.

Published in final edited form as:

Int J Radiat Oncol Biol Phys. 2021 June 01; 110(2): 526–538. doi:10.1016/j.ijrobp.2020.12.035.

IGF-1 receptor signaling regulates type II pneumocyte senescence and resulting macrophage polarization in lung fibrosis.

Eun Joo Chung, PhD[1], **Seokjoo Kwon, PhD**[1], **Jessica L. Reedy, PhD**[1], **Ayla O. White, BSc**[1], **Joon Seon Song, MD. PhD**[2,3], **Ilseon Hwang, MD. PhD**[2,4], **Joon Yong Chung, PhD**[2], **Kris Ylaya, BSc**[2], **Stephen M. Hewitt, MD. PhD**[2], **Deborah E. Citrin, MD**[1,*]

[1]Radiation Oncology Branch, Center for Cancer Research, National Cancer Institute, National Institutes of Health, Bethesda, MD, USA.

[2]Experimental Pathology Laboratory, Laboratory of Pathology, Center for Cancer Research, National Cancer Institute, National Institutes of Health, Bethesda, MD, USA.

[3]Department of Pathology, Asan Medical Center, University of Ulsan College of Medicine, Seoul, Republic of Korea.

[4]Department of Pathology, Keimyung University School of Medicine, Dongsan Medical Center, Daegu, Republic of Korea.

Abstract

Background—Type II pneumocyte (AECII) senescence has been implicated in the progression of lung fibrosis. The capacity of senescent cells to modulate pulmonary macrophages to drive fibrosis is unexplored. Insulin-like growth factor-1 receptor (IGF-1R) signaling has been implicated as a regulator of senescence and aging.

Methods—Mice with an AECII specific deletion of IGF-1R received thoracic irradiation (n≥5 per condition) and the effect of IGF-1R deficiency on radiation-induced AECII senescence and macrophage polarization to an alternatively activated phenotype (M2) was investigated. IGF-1R

[*]**Corresponding author:** Deborah Citrin, M.D., Radiation Oncology Branch, Center for Cancer Research, National Cancer Institute, National Institutes of Health, 10 Center Dr. Building 10 CRC, B2-3500, Bethesda, MD 20892, USA. Phone: 301-496-5457. Fax: 301-480-5439. citrind@mail.nih.gov.

Author contributions: Eun Joo Chung, and Seokjoo Kwon were involved in study design, acquiring data, analyzing data, and writing the manuscript. Ayla O. White and Kris Ylaya participated in acquiring data. Jessica L. Reedy was involved in writing the manuscript. Joon Seon Song, Ilseon Hwang, Joon Yong Chung, and Stephen M. Hewitt were analyzed and interpreted clinical and IHC data. Deborah E. Citrin was involved in study design, analyzing data, and writing the manuscript. **Statistical analysis** was performed by Eun Joo Chung (chuneu@mail.nih.gov).

Disclosures: None

Data availability: All gene expression data generated and analyzed during this study are included in this published article and its supplementary information files.

Conflict of Interest Statement: The authors have no conflict of interest to declare regarding the publication of this article.

signaling, macrophage polarization, and senescence were evaluated in surgically resected human lung (n=63).

Results—IGF-1R deficient mice demonstrated reduced AECII senescence (senescent AECII/field; intact: 7.25[average] ± 3.5[SD] %, deficient: 2.75 ± 2.8 %, p=.0001), reduced accumulation of M2 macrophages (intact: 24.7 ± 2.2 cells/field, deficient: 15.5 ± 1.2 cells/field, p=.0086), and fibrosis (hydroxyproline content; intact: 71.9 ± 21.7 μg/lung, deficient: 31.7 ± 7.9, p=.0485) after irradiation. Senescent AECII enhanced M2 polarization in a paracrine fashion (relative *Arg1* mRNA, 0 Gy: 1.0 ± 0.4, 17.5 Gy: 7.34 ± 0.5, p<.0001). Evaluation of surgical samples from patients treated with chemo-radiation demonstrated increased expression of IGF-1 (unirradiated: 10.2 ± 4.9 % area, irradiated: 15.1 ± 11.5 %, p=.0377), p21 (unirradiated: 0.013 ± 0.02 histoscore, irradiated: 0.084 ± 0.09 histoscore, p=.0002), IL-13 (unirradiated: 13.7 ± 2.8 % area, irradiated: 21.7 ± 3.8 %, p<.0001), and M2 macrophages in fibrotic regions relative to non-fibrotic regions (unirradiated: 11.4 ± 12.2 CD163+ cells/core, irradiated: 43.1 ± 40.9 cells/core, p=.0011), consistent with findings from animal models of lung fibrosis.

Conclusion—This study demonstrates that senescent AECII are necessary for the progression of pulmonary fibrosis and serve as a targetable, chronic stimuli for macrophage activation in fibrotic lung.

Introduction

Lung irradiation during therapy for thoracic malignancies can result in pneumonitis and pulmonary fibrosis. Cellular senescence is implicated in the progression of pulmonary fibrosis of multiple etiologies (1–4). Alveolar epithelial cells Type II (AECII) are surfactant producing cells that also function as alveolar stem cells after lung injury, repopulating both AECII and AECI. Pulmonary injuries that culminate in fibrosis are accompanied by senescence and progressive depletion of AECII (2,5,6). The impact of senescence in the relatively small AECII compartment on the progression of fibrosis and the inflammatory milieu of the lung has not been evaluated.

Activation of the IGF-1 signaling pathway has been implicated in modulation of cellular senescence and aging in normal tissues, including senescence after irradiation (7–9). Prolonged IGF-1 exposure in primary cells and fibroblasts induces cellular senescence via p53 stabilization and SIRT1 inhibition (10,11). Deletion or inhibition of the IGF-1 receptor has been demonstrated to prevent cellular senescence, reduce aging in tissues, and extend lifespan in organisms (12–15).

We hypothesized that selectively preventing AECII senescence would ameliorate fibrotic progression following irradiation. To test this hypothesis, we exposed mice with AECII specific *Igf1r* conditional deletion to thoracic irradiation. *Igf1r* deficient mice exhibited markedly reduced AECII senescence, fibrosis, and accumulation of alternatively activated macrophages after irradiation compared to control mice. Interleukin-13 (IL-13) secreted by senescent AECII was capable of polarizing macrophages towards an alternative phenotype. Concordant findings of increased expression of IGF-1, p21, IL-13, and accumulation of alternatively activated macrophages were observed in irradiated human lung tissue. These data indicate that IGF-1R signaling is necessary for AECII senescence, and that prevention

of AECII senescence is sufficient to mitigate radiation-induced macrophage polarization and fibrotic progression.

Materials and methods

Mice and irradiation

Animal procedures were approved by the Animal Care and Use Committee (National Cancer Institute, Bethesda, MD) and in accordance with the guidelines of the Institute of Laboratory Animal Resources, National Research Council. Additional elements of the ARRIVE guidelines for reporting of animal studies are included in the Supplementary Methods (16). To inactivate IGF-1 signaling selectively in AECII, B6;129-*Igf1r*^{tm2Arge}/J mice (Jackson Laboratories, Bar Harbor, ME) and B6.129S-*Sftpc*$^{tm1(cre/ERT2)Blh}$/J mice (a kind gift of Brigid Hogan, Duke University) were crossbred (Supplementary Methods). Eight-week old F2 progeny (*Igf1r*$^{flx/flx}$; *Spc-Cre*^{ERT2}) received corn oil (vehicle) or tamoxifen (200 mg/kg) 3 times per week (n≥8 per condition). Two weeks after the last injection, mice received thoracic irradiation (five daily fractions of 6 Gy) with an X-RAD 320 (Precision X-Ray, North Branford, CT) using 2.0 mm Al filtration (320 kv peak) at a dose rate of 1.9 Gy/min. At the indicated timepoints, lung was snap frozen and stored at −80°C, inflated with 10 % neutral buffered formalin and paraffin embedded, or processed for frozen sections.

Histopathology

Formalin-fixed paraffin-embedded (FFPE) lung sections were deparaffinized in xylene, rehydrated, and stained with hematoxylin and eosin (H&E) or Masson's trichrome stain (Sigma-Aldrich, St Louis, MO). Stained lung was examined on a Leica DMRXA microscope (Wetzlar, Germany). Digital micrographs were captured at 10x magnification using a QImaging Micropublisher Camera (Surrey, BC, Canada).

Hydroxyproline Assay

Hydroxyproline content was measured using a Hydroxyproline assay (Sigma-Aldrich) according to the manufacturer's protocol and expressed as micrograms per lung.

Quantitative PCR

Total RNA from frozen murine tissue was extracted with Trizol reagent (Life Technologies) and purified with the RNeasy plus system (Qiagen, Valencia, CA), and 150–500 ng of purified RNA was reverse-transcribed using QuantiTect reverse transcription kit (Qiagen). Total RNA from human FFPE sections was extracted using the High Pure RNA Paraffin kit (Roche Diagnostic, Mannheim, Germany), and 1μg of RNA was reverse-transcribed as described above. Quantitative PCR (qPCR) was performed on an ABI 7500 system (Applied Biosystems) using predesigned primer and probe sets for Taqman gene expression assays (Life Technologies, Grand Island, NY) and normalized to actin.

Senescence assay

Lung sections or primary cell cultures were incubated with anti-prosurfactant protein C antibody (Abcam, Cambridge, MA) after β-galactosidase activity assay (Abcam,

Cambridge, MA), and treated with a secondary antibody conjugated to Alexa Flour 594 (Life Technologies, Grand Island, NY). Slides were mounted with ProLong antifade reagent containing DAPI (Life Technologies, Grand Island, NY). The number of senescent AECII was counted on five 20x fields per mouse (n≥5).

Cell isolation

Pulmonary cell subsets were isolated from C57BL/6J and *Igf1r*; *Spc-Cre*^{ERT2} mice, as previously described (2) and as detailed in the Supplementary Methods.

Enzyme-linked immunosorbent assay

Lung homogenates were prepared with ice-cold T-Per buffer (Thermo Scientific, Waltham, MA) containing 1x Halt Protease and Phosphatase inhibitor cocktail (Thermo Scientific). Equal protein concentrations were used for ELISA sandwich assays (R&D Systems, Minneapolis, MN) performed according to the manufacturer's protocol.

Bone marrow derived macrophage cultures

Monocytes were enriched from C57BL/6J bone marrow, pre-differentiated into macrophages by 6-day culture in RPMI/10 % FCS supplemented with 20 ng/ml of M-CSF, then cultured with AECII conditioned media (CM). Briefly, primary AECII were enriched from C57BL/6J, irradiated with 17.5 Gy, and treated with 3 μM ABT-263 (Selleckchem, Houston, TX) or vehicle for 24 hours beginning 48 hours after irradiation. AECII cultures were then triple washed and conditioned with serum-reduced media (0.5 % FBS) for 16 hours. In additional studies, macrophages cultures were treated with AECII conditioned media and an IL-13 neutralizing antibody (1 μg/ml, MAB413, R&D System) or isotype control for 24 hours.

Flow cytometry

Single cell suspensions were produced from murine lung (n≥5) after irradiation. After blocking the Fc receptor with anti-mouse CD16/CD32 antibody (101335), cells were labeled with fluorophore-conjugated BioLegend antibodies against mouse CD11b (101217), CD206 (141726), and F4/80 (123116). Labeled cells were fixed with 2 % PFA and acquired 100,000 events for each sample with LSR Fortessa (BD Biosciences, Franklin Lakes, NJ) and analyzed with FloJo (Tree Star, Inc., Ashland, OR).

IHC profiling of human lung tissue

Lung tissue from 63 patients was acquired at the time of surgical resection for the management of non-small cell lung cancer at Asan Medical Center between between 2005 and 2017. This study was approved by the Regional Institutional Review Board of Asan Medical Center (approval no. 2020– 0566). All irradiated patients (n=34) received 45 Gy in 25 fractions. Additional clinicopathologic details are described in Supplementary Table 1. Assessment of specimens to confirm freedom from visible tumor and scoring of fibrosis was conducted by two pathologists (JSS and IH).

TMA construction and IHC profiling of human lung tissue

Fibrotic and normal regions were selected from hematoxylin and eosin (H&E) and Masson's trichrome stained slides. Using a 1-mm diameter tissue cylinder, two cores were taken from each FFPE tissue block and transplanted into recipient blocks using a tissue arrayer (Beecher Instruments, Inc., Silver Spring, MD).

TMA sections at 5 μm thickness were deparaffinized in xylene and rehydrated through a graded alcohol series. Antigen retrieval was performed in citrate buffer (murine lung: pH 6.0, Vector Labs, Burlingame, CA; human lung: pH 9.0, Dako, Carpinteria, CA) at 125 °C, 15–17 Pa for 30 seconds in a Pascal Pressure cooker (Dako, Carpinteria, CA). Endogenous peroxidase was quenched with 0.3 % H_2O_2 for 10 minutes. Sections were blocked with 2.5 % normal horse serum for 1 hour and incubated with primary antibodies at 4°C overnight. Primary immunoreactivity was detected with a polymeric peroxidase-conjugated secondary antibody (ImmPress, Vector Labs) and visualized by 3,3'-diaminobenzidine histochemistry (ImmPACT, Vector) in murine lung sections, and with Envision+ detect system (Dako) and 3,3'-diaminobenzidine (DAB) in patient lung tissues. Sections were counterstained with Gill's Hematoxylin (Sigma-Aldrich), dehydrated, and mounted with Permount. Anti-mouse IGF-1 (ab40657), anti-mouse IGF-2 (ab9574), anti-mouse p21 (ab107099) anti-mouse F4/80 (ab6640) and anti-mouse Arginase-1 (ab11884) antibodies were purchased from Abcam (Cambridge, MA). Anti-human IGF-1 (HPA048946), anti-human p21 (2947), anti-human IL-13 (ab106731) and anti-Cre antibody (908002) were purchased from Sigma Aldrich (St. Louis, MO), Cell Signaling Technology (Danvers, MA), Abcam and BioLegend (San Diego, CA). Anti-phospho-IGF-1R (ab39398, Abcam) and anti-pro-SPC (sc-7705, Santa Cruz Biotechnology (Dallas, TX) were utilized for immunofluorescence, and visualized with fluorophore-conjugated secondary antibodies (Thermo Fisher, Waltham, MA). Labeled sections were counterstained with 4',6-diamidino-2-phenylindole (DAPI, Sigma Aldrich) and mounted with Prolong Gold Anti-Fade Reagent (Life Technologies, Carlsbad, CA).

Digital image analysis.

Stained TMA slides were scanned with an Aperio AT2 digital scanner (v) in 20x objective magnification and the images were automatically analyzed using Visiopharm software v6.9.1 (Visiopharm, Hørsholm, Denmark).

NanoString assays

Total RNA extracted from FFPE sections using the High Pure RNA Paraffin kit (Roche Diagnostic) was quantified using the DS-11 spectrophotometer (DeNovix, Wilmington, DE), and evaluated on the Bioanalyzer (Agilent Technologies, Santa Clara, CA) using DV200 as an indicator of RNA quality (Supplementary Table 2).

Expression of mRNA was assessed using a customized CodeSet containing probes against target genes related to senescence, inflammation and fibrosis (Supplementary Table 3) according to the manufacturer's instructions. Briefly, probes and 100 ng total RNA from each sample were hybridized overnight at 65°C according to the manufacturer's protocol. A NanoString nCounter Digital Analyzer (NanoString Technologies, Seattle, WA) was used to count the digital barcodes representing the number of transcripts. The raw expression data

were normalized using nSolver Analysis software. A normalization factor was calculated by obtaining the geometric mean of the positive controls used for each sample and applied to the raw counts of the nCounter output data to eliminate variability that was unrelated to the samples. The resulting data were normalized again with the geometric mean of the housekeeping genes.

Statistical Analyses

Data are presented as mean ± standard deviation unless otherwise noted. Statistical analyses were performed using either Mann-Whitney test (non-parametric statistical test) for comparisons between two conditions or ANOVA with Tukey's correction for multiple comparisons. A p value of ≤0.05 was considered significant for comparisons. All studies in tissues were conducted in triplicate unless otherwise noted.

Results

Senescence markers in murine pulmonary injury after irradiation

Expression of $p16^{Ink4a}$ is commonly used as marker of senescence, however prior studies have suggested that $p16^{Ink4a}$ promotor activation may decline over time (17) and that other cell types, such as macrophages may exhibit $p16^{Ink4a}$ expression (18). To confirm the most appropriate marker for senescence in current model, primary AECII isolated from mouse lung were irradiated *in vitro* with 17.5 Gy, a dose of radiation previously demonstrated to induce senescence in AECII (2). The percent of AECII with β-Galactosidase activity was increased after irradiation (0 Gy: 10.7 ± 2.16 %, 17.5 Gy: 19.6 ± 3.64 %, p=.0111), as was the relative expression of *p21* (0 Gy: 1.0 ± 0.05, 17.5 Gy: 3.46 ± 0.14, p=.0112) and *Igf1* mRNA (0 Gy: 1.0 ± 0.04, 17.5 Gy: 1.63 ± 0.64, p=.0111), but not *p16Ink4a* mRNA (0 Gy: 1.0 ± 0.07, 17.5 Gy: 0.89 ± 0.11, p=.4224), (Supplementary Figure 1A–D). Analysis of AECI, AECII, and macrophages isolated from murine lungs after thoracic irradiation revealed significantly increased *p21* mRNA expression in AECII after irradiation (0 Gy: 1.31 ± 0.03, 5×6 Gy: 2.14 ± 0.12, p=.0120) (Supplementary Figure 1F). In contrast, *p16Ink4a* mRNA expression was significantly increased only in macrophages (0 Gy: 2.14 ± 0.06, 5×6 Gy: 3.09 ± 0.13, p=.0003) (Supplementary Figure 1E), suggesting that *p16Ink4a* mRNA expression is not highly specific for epithelial senescence in this model.

Increased IGF-1 expression in AECII after irradiation

Prolonged IGF-1 exposure is known to induce cellular senescence (10). To evaluate IGF-1 signaling after IR, C57BL/6J mice were treated with 5 daily fractions of 6 Gy thoracic IR, a previously validated radiation regimen (2). IGF-1 concentrations in lung were significantly increased at 16 weeks after irradiation relative to age matched unirradiated lung (0 Gy: 1472.3 ± 51.5 pg/ml, 5×6 Gy: 2591.6 ± 333.1 pg/ml, p=.0013) (Figure 1A), whereas IGF-2 concentrations increased only as a function of age (2 week: 16.1 ± 6.4 pg/ml, 16 week: 59.5 ± 10.7 pg/ml, p=.0044) (Figure 1B). IGF-1 receptor (IGF-1R) phosphorylation was elevated in irradiated lung compared to age-matched normal lung (Figure 1C), consistent with activation of IGF signaling. Irradiation increased the relative expression of *Igf1* mRNA in AECII (0 Gy: 2.12 ± 0.02, 17.5 Gy: 3.03 ± 0.05, p=.0001) primary cultures, but not AECI (0 Gy: 1.0 ± 0.016, 17.5 Gy: 1.20 ± 0.006, p=.0610) (Figure 1D). IGF-1 neutralization

was sufficient to prevent radiation-induced senescence in primary AECII cultures (isotype-control: 19.6 ± 3.7 %, anti-IGF1antibody: 7.73 ± 1.6 %, p=.0021) (Figure 1E). These findings demonstrate a role of IGF-1R signaling in AECII senescence after IR.

Deficiency of IGF-1R in AECII protects against radiation-induced lung injury.

To inactivate IGF-1 signaling selectively in AECII, *Sftpc-CreER*^{T2} mice expressing a tamoxifen-inducible Cre recombinase at the *Sftpc* locus (B6.129S-*Sftpc*$^{tm1(cre/ERT2)Blh}$/J; Jackson Laboratory) were crossed with mice possessing loxP sites in the IGF-1 receptor gene (Igf1r) (B6;129-*Igf1r*^{tm2Arge}/J; Jackson Laboratory). F2 progeny homozygous for both alleles (*Igf1r*$^{flx/flx}$ /*Spc-Cre*$^{+}$) were treated with Tamoxifen for specific deletion of IGF-1R in AECII or vehicle (corn oil; Supplementary Figure 2). Lungs from vehicle treated *Igf1r* $^{flx/flx}$/*Spc-Cre*$^{+}$ mice exhibited extensive fibrosis (Figure 2A & B) and hydroxyproline accumulation after irradiation (intact: 0 Gy: 30.9 ± 7.6 μg/lung, 5×6 Gy: 71.9 ± 21.7 μg/lung, p=.0218) (Figure 2C). In contrast, tamoxifen treated, irradiated *Igf1r* $^{flx/flx}$/*Spc-Cre*$^{+}$ mice developed markedly attenuated pulmonary fibrosis with no significant in hydroxyproline content (deficient; 0 Gy: 26.0 ± 10.4 μg/lung, 5×6 Gy: 37.1 ± 7.9 μg/lung, p=.7402). IGF-1R deficiency led to significantly reduced AECII senescence (senescent/total AECII; intact: 7.25 ± 3.5 %, deficient: 2.75 ± 2.8 %, p=.0001) (Figure 2D) and depletion (pro-SPC+/field; intact: 0.79 ± 0.2 cells/field, deficient: 1.11 ± 0.3 cells/field, p=.0275) (Figure 2E) compared to mice with intact IGF-1R. These findings further support the notion that IGF-1R signaling in AECII contributes to senescence and lung fibrosis.

Alternatively activated macrophages are the dominant immune cell observed in fibrotic lung after irradiation (19–22). Mice with IGF-1R deficiency in AECII exhibited reduced pulmonary macrophage accumulation (F4/80+/field; intact: 28.0 ± 7.1 cells/field, deficient: 19.8 ± 8.1 cells/field, p=.0050) (Figure 2F–G) and dramatically reduced accumulation of Arg-1 positive cells (Arg-1+/field; intact: 24.8 ± 5.4 cells/field, deficient: 7.5 ± 2.9 cells/field, p<.0001) (Figure 2F & H) after irradiation compared to vehicle treated *Igf1r* $^{flx/flx}$/*Spc-Cre*$^{+}$ mice. Flow cytometry of single cell suspensions prepared from *Igf1r* $^{flx/flx}$/*Spc-Cre*$^{+}$ lungs (Figure 3A) demonstrated a significant increase in infiltrating (CD11b+, F4/80+, CD206+) and residential (CD11b-, F4/80+, CD206+) macrophages at 16 weeks after irradiation in mice with intact IGF-1R, an effect that was diminished with IGF-1R deficiency in AECII ([infiltrating; intact: 32.6 ± 7.2 %, deficient: 13.5 ± 2.8 %, p<.0001], [residential; intact: 7.69 ± 0.9 %, deficient: 3.55 ± 1.4 %, p=.0002]) (Figure 3 B–D) or with senolytic therapy ([infiltrating; vehicle: 16.2 ± 3.9 %, ABT263: 5.8 ± 0.5 %, p=.0281], [residential; vehicle: 1.82 ± 0.4 %, ABT263: 0.02 ± 0.01 %, p=.0167]) (Supplementary Figure 3).

Senescent AECII contribute to M2 macrophage polarization via IL13 secretion.

These findings suggest that senescent AECII contribute to the accumulation of alternatively activated macrophages (M2) after irradiation. To investigate if the observed macrophage polarization was related to IGF-1 signaling and senescence in AECII, primary AECII were enriched from *Igf1r* $^{flx/flx}$/*Spc-Cre*$^{+}$ mice treated with vehicle or Tamoxifen, irradiated, and treated with ABT263 (a senolytic agent) (Figure 4A). Conditioned media from AECII cultures was applied to bone marrow derived macrophages (BMDM). Radiation-induced

senescence in AECII was reduced with either IGF-1R deficiency or senolytic treatment (senescent/total AECII; [intact-17.5 Gy: 51.8 ± 6.8 %, deficient-17.5 Gy: 17.9 ± 6.3 %, p=.0017], [intact-17.5 Gy vehicle: 51.8 ± 6.8 %, intact-17.5 Gy ABT263: 7.5 ± 6.6 %, p=.0002]) (Figure 4B). BMDM exposed to conditioned media from irradiated AECII with intact IGF-1R displayed a significant increase in *Arg1* mRNA expression (intact 0 Gy-CM: 1.0 ± 0.5 relative expression, intact 17.5 Gy-CM: 7.34 ± 0.5 relative expression, p<.0001) (Figure 4C) and relative expression of *Cd206* mRNA (intact 0 Gy-CM: 1.0 ± 0.06, intact 17.5 Gy-CM: 3.74 ± 2.1, p=.0074) (Supplementary Figure 4). In contrast, BMDM exposed to conditioned media from irradiated IGF-1R deficient AECII, or irradiated IGF-1R intact AECII treated with ABT-263 did not express markers of alternative activation (IGF-1R deficiency; 0 Gy-CM: 1.68 ± 0.02 relative expression, deficient 17.5 Gy-CM: 2.57 ± 0.59 relative expression, p=.1756) (senolytic treatment; 0 Gy-ABT-263 CM: 1.1 ± 0.08, 17.5 Gy-ABT-263 CM: 1.59 ± 0.4, p=.3416). These findings support the hypothesis that senescence drives the elaboration of molecules by AECII that are capable of altering macrophage phenotype.

Il13 expression in primary AECII cultures was evaluated as a contributing paracrine factor (Figure 4D). Irradiation increased *Il13* mRNA expression in IGF-1R competent AECII (intact-0 Gy: 1.0 ± 0.45, intact-17.5 Gy: 3.9 ± 0.35, p=.0001), whereas deficiency of IGF-1R (deficient-0 Gy: 0.6 ± 0.19, deficient-17.5 Gy: 0.8 ± 0.39, p=.9898) or treatment with ABT-263 (intact-0 Gy-ABT263: 0.01 ± 0.01, intact-17.5 Gy-ABT263: 1.10 ± 0.37, p=.0553) was capable of preventing radiation-induced *Il13* m RNA expression. Further, neutralization of IL-13 was sufficient to prevent the capacity of irradiated AECII conditioned media to polarize BMDM towards an Arg-1 (relative *Arg1* mRNA: isotype-control 17.5 Gy: 4.01 ± 0.40, anti-IL13 antibody17.5 Gy: 1.85 ± 0.04, p=.0012) (Figure 4E) and CD206 (relative *Cd206* mRNA: isotype-control 17.5 Gy: 4.42 ± 1.63, anti-IL13 antibody17.5 Gy: 1.99 ± 1.08, p=.0224) (Supplementary Figure 4C) expressing phenotype. Collectively, these data suggest that senescent AECII contribute to alternative activation of macrophages through elaboration of IL-13.

Differential gene expression in irradiated human lungs.

To confirm that pathways identified in the murine model were relevant to the human condition, the expression of genes implicated in senescence, fibrosis, and aging were compared between samples of 13 patients with unirradiated, histologically normal pulmonary parenchyma and samples from 30 patients with irradiated lung (Figure 5A). Unsupervised hierarchical clustering based on gene expression revealed two distinguishable groups, one consisting of 13 unirradiated and 4 irradiated specimens, and another which consisted of 26 irradiated specimens (Figure 5B). Of the 414 genes analyzed, 174 genes were differentially expressed between unirradiated and irradiated lung ($p<0.05$), including *IGF1* (Supplementary Figure 5).

Restricting the clustering analysis to genes implicated in fibrosis again resulted in separate grouping of irradiated and unirradiated samples (Figure 5C). Consistent with the murine model, the expression of *IGF1* (unirradiated: 38.3 ± 15.9 Log_2 Ct, irradiated: 116.7 ± 86.8, p=.0156), but not *IGF2* (unirradiated: 71.4 ± 28.8 Log_2 Ct, irradiated: 145.0 ±

110.1, p=.1677), was increased significantly in irradiated human lung samples (Figure 5D). Quantitative PCR was used to validate increased expression of selected fibrosis related genes and *IGF1* in human lung tissue after radiotherapy. As shown in Supplementary Figure 5B, mRNA levels of *IGF1*, *CCL2*, *COL1A2*, *COL3A1*, and *COL5A1* were increased significantly in response to irradiation. The relative levels of *ACTA2* mRNA were increased in irradiated lung tissue but did not meet the threshold of significance.

IGF-1 expression and senescence in irradiated human lung

Further studies were conducted in custom TMAs composed of 126 cores (2 cores per specimen) of surgically resected human lung tissue from patients with chemo-radiotherapy (n=34) or without (n=29). Histological changes were assessed in TMA sections after Masson Trichrome stain, with fibrotic regions only found in irradiated lung cores (Figure 6A). IGF-1 expression was significantly increased in irradiated lung tissue from both fibrotic and non-fibrotic regions relative to that observed in samples from unirradiated lung (unirradiated: 10.2 ± 4.9 % area, irradiated: 15.1 ± 11.5 % area, p=.0377) (Figure 6B). The expression of p21 was similarly increased significantly in irradiated lungs compared to unirradiated lungs (unirradiated: 0.013 ± 0.02 histoscore, irradiated: 0.084 ± 0.09 histoscore, p=.0002) (Figure 6C), with the highest expression observed in fibrotic regions. IL-13 expression was often patchy within TMA cores, with a notable increase in fibrotic samples (unirradiated: 13.7 ± 2.8 % area, irradiated: 21.7 ± 3.8 % area, p<.0001) (Figure 6D). A significant accumulation of cells expressing CD68 (pan-macrophage marker) (CD68+ cells/core, unirradiated: 52.5 ± 38.7, irradiated: 84.3 ± 70.4 cells/core, p=.0453) and CD163 (M2 macrophage marker) (CD163+ cells/core, unirradiated: 11.4 ± 12.2, irradiated: 43.1 ± 40.9, p=.0003) was found in irradiated lung tissues compared to unirradiated controls (Figure 6E&F). These findings suggest that the murine model of radiation lung injury shares relevant similarities with the human condition in the context of IGF-1 expression, senescence, and alternative macrophage accumulation.

Discussion

In this study we demonstrate that IGF-1R signaling and resulting senescence in AECII is a key factor in pulmonary fibrosis after radiation. We demonstrate that IL-13 secretion by senescent AECII contributes to macrophage polarization towards an alternatively activated phenotype. We further confirm that the findings of increased IGF-1 expression and accumulation of alternatively activated macrophages are found in human lung tissue exposed to radiation.

Pulmonary fibrosis resulting from diverse diseases, including idiopathic fibrosis, scleroderma, infections, and exposure to radiation or other toxic stimuli has been linked to senescence in lung (1–4). One method commonly used to study the impact of senescent cells in tissue is transgenic mouse models that allow for the inducible removal of $p16^{Ink4a}$-positive senescent cells, such as the INK-ATTAC and p16–3MR strains (1,23). There is no universal marker of senescence, however $p16^{Ink4a}$ is commonly expressed in a variety of senescent cells (17). Recent work has also demonstrated that alternatively activated macrophages, which contribute to pulmonary fibrosis (24–26), express markers

of senescence, including $p16^{Ink4a}$ and β-Galactosidase (18,27). Thus, it has been postulated that at least some of the benefit observed in studies using mouse models in which senescent cell clearance is dependent on $p16^{Ink4a}$ expression may be due to clearance of profibrotic macrophages (18,27).

Another method for studying the impact of senescent cells in disease is the delivery of senolytic agents that are capable of selectively clearing senescent cells. These agents often have additional targets and a mechanism of action that may complicate the interpretation of the relative contribution of senolytic action to any observed benefit. We sought to employ a method that would clarify the impact of preventing senescence selectively in the relatively rare AECII cells to clarify the role of stem cell senescence in fibrotic progression.

We noted that deficiency of IGF-1R in AECII not only prevented the accumulation of senescent AECII after radiation, but also reduced the accumulation of residential and infiltrating monocyte-derived M2 macrophages, suggesting a link between the two processes. Chronic and persistent elaboration of the senescence-associated secretory phenotype (SASP) by senescent cells has been implicated in senescence-related pathology (28,29). The capacity of senescent AECII to polarize macrophages toward the M2 phenotype was dependent on IL-13, a component of the SASP (30) that is known to polarize macrophages towards an M2 phenotype and play a critical role in fibrotic progression (19,31,32). Our study suggests that senescent cells may contribute to fibrosis by promoting macrophage polarization towards a pro-fibrotic M2 phenotype in lung after irradiation.

Prior studies have demonstrated the importance of monocyte-derived macrophages relative to tissue resident alveolar macrophages in fibrotic progression (24). Our findings are consistent with prior studies demonstrating accumulation of alternatively activated macrophages in the presence of senescent cells (18,27), however the reason for this correlation was previously unclear. Both IGF-1R deficiency and senolytic therapy were capable of reducing the accumulation of monocyte derived macrophages in our study. A unique aspect of this study is the use of a genetically engineered model not dependent on $p16^{Ink4a}$ to reduce senescence in tissues. As $p16^{Ink4a}$ based clearance may also clear alternatively activated macrophages, the interaction between these two cell subsets with demonstrated roles in pulmonary fibrosis has been challenging to decipher.

These studies demonstrate that $p16^{Ink4a}$ may not be an optimal marker for senescence in radiation injury models. The expression of $p16^{Ink4a}$ is dynamic after senescence inducing stimuli (17) and also increase with age (33). Recently it has been suggested that activation of the $p16^{Ink4a}$ promoter occurs at the time of cell cycle arrest and later decreases (17). In this model, $p16^{Ink4a}$ expression was primarily localized to alveolar macrophages and was discordant to p21 expression and SA β-Gal activity. Given the long duration (4–6 months) of radiation injury models, it is possible that an initial $p16^{Ink4a}$ expression in AECII is diminished at later time points. Regardless, these data suggest that p21 and SA β-Gal may be preferable markers in chronic radiation injury models for lung which are dominated by tissue residential macrophages and suggest that $p16^{Ink4a}$ promotor elimination strategies may serve to primarily clear macrophages in chronic radiation injury models. Further study

is required to clarify the kinetics of $p16^{Ink4a}$ promotor activity in the various cell types present in lung after irradiation.

IGF-1 signaling can play conflicting roles in tissue homeostasis (9). IGF-1 signaling functions to enhance cell proliferation and survival in healthy tissue (34,35). Conversely, activation of the IGF-1 pathway after irradiation has been linked to senescence in primary cells (8). The role of IGF-1 signaling in the balance of senescence and apoptosis after DNA damage may also be impacted by p53 status (10,36). Indeed, studies in tumor cells have demonstrated that inhibiting IGF-1R signaling sensitizes to radiation and increases apoptosis (37–40).

The timing of IGF-1 signaling activation and inhibition may also play a role in the conflicting nature of studies, whereas inhibition of IGF-1R pathway activation prior to irradiation prevents senescence, but inhibition after the presence of established senescence results in apoptosis. The cause for these conflicting cellular responses is not known, but may be related to the dependence of senescent cells on anti-apoptotic factors such as bcl-2 and soluble Clusterin (7,41), molecules known to be induced by IGF-1 pathway activation after injury or senescence (7,42). Further, the balance of apoptosis and senescence after cellular stress, such as irradiation, is cell-type specific (43), potentially complicating extrapolation of findings in other organs to lung.

This study has some limitations. IGF-1 signaling has been implicated in the progression of pulmonary fibrosis in human IPF tissue and in murine models (44,45). Studies evaluating the importance of IGF-1 signaling have typically utilized IGF-1R inhibition, potentially exposing other cell types to IGF-1R inhibition, including macrophages, which are known to be dependent on IGF-1R signaling to maintain M2 polarization (46). In an effort to minimize the confounding impact on other cell types in lung from systemic IGF-1R inhibition, we generated a mouse model in which IGF-1R was selectively deleted in AECII. It is conceivable that some of the effects we observed *in vivo* and *in vitro* were related to impaired IGF-1R signaling and not due to prevention of senescence. To address this weakness, we confirmed out findings with a senolytic agent that does not impact IGF-1R signaling and found similar effects as those observed with IGF-1R deficiency.

A weakness of many studies investigating the mechanism of lung fibrosis is the absence of human tissue for validation. We confirmed our key findings in human lung tissue collected at the time of surgery. Some assays that would further validate our findings are not feasible using fixed tissue. Thus, in future studies, evaluating fresh tissue may provide additional experimental evidence and allow deeper mechanistic insight. The tissue that was studied was collected from patients with lung cancer several weeks following treatment, as this timing of surgery is the current standard of care. Special care was taken to avoid tumor bearing regions in the resected specimen to minimize the chance that tumor specific paracrine effects could be impacting our studies. Finally, we have focused on the role of IL-13 production by senescent AECII, as IL-13 is a driver of alternative activation of macrophages and plays a key role in lung fibrosis (19,31,32,47,48). Senescent cells are known to secrete numerous cytokines and molecules as part of the SASP (30), and it is likely that additional secreted factors play a key role in post-injury lung fibrosis.

Our studies strongly support the hypothesis that senescent AECII play a critical role in fibrotic progression, including a capacity to polarize macrophages to a pro-fibrotic M2 phenotype. Future studies will focus on identifying addition factors in the SASP that contribute to the profibrotic environment through interaction with macrophages or other cell types. These findings also support investigations of replenishing AECII via stem cell therapy as a method to rescue lungs after exposure to pro-fibrotic stimuli. As AECII serve as an alveolar stem cell, understanding how to most effectively prevent or clear senescent cells without harming stem cell reserve is a critical scientific goal moving forward.

Supplementary Material

Refer to Web version on PubMed Central for supplementary material.

Acknowledgement:

This research was supported by the Intramural Research Program of the National Institutes of Health, National Cancer Institute.

Funding: This research was supported by the Intramural Research Program of the CCR, NCI, NIH (ZIA BC 010850).

References

1. Schafer MJ, White TA, Iijima K, et al. Cellular senescence mediates fibrotic pulmonary disease. Nat Commun 2017;8:14532. [PubMed: 28230051]
2. Citrin DE, Shankavaram U, Horton JA, et al. Role of type II pneumocyte senescence in radiation-induced lung fibrosis. J Natl Cancer Inst 2013;105:1474–1484.. [PubMed: 24052614]
3. Alder JK, Chen JJ, Lancaster L, et al. Short telomeres are a risk factor for idiopathic pulmonary fibrosis. Proc Natl Acad Sci U S A 2008;105:13051–6. [PubMed: 18753630]
4. Minagawa S, Araya J, Numata T, et al. Accelerated epithelial cell senescence in IPF and the inhibitory role of SIRT6 in TGF-beta-induced senescence of human bronchial epithelial cells. Am J Physiol Lung Cell Mol Physiol 2011;300:L391–401. [PubMed: 21224216]
5. Evans MJ, Cabral LJ, Stephens RJ, et al. Transformation of alveolar type 2 cells to type 1 cells following exposure to NO2. Exp Mol Pathol 1975;22:142–50. [PubMed: 163758]
6. Fehrenbach H. Alveolar epithelial type II cell: Defender of the alveolus revisited. Respir Res 2001;2:33–46. [PubMed: 11686863]
7. Luo X, Suzuki M, Ghandhi SA, et al. ATM regulates insulin-like growth factor 1-secretory clusterin (IGF-1-sCLU) expression that protects cells against senescence. PLoS One 2014;9:e99983.
8. Panganiban RA, Day RM. Inhibition of IGF-1R prevents ionizing radiation-induced primary endothelial cell senescence. PLoS One 2013;8:e78589.
9. Day RM, Snow AL, Panganiban RA. Radiation-induced accelerated senescence: A fate worse than death? Cell Cycle 2014;13:2011–2. [PubMed: 24922064]
10. Tran D, Bergholz J, Zhang H, et al. Insulin-like growth factor-1 regulates the SIRT1-p53 pathway in cellular senescence. Aging Cell 2014;13:669–78. [PubMed: 25070626]
11. Handayaningsih AE, Takahashi M, Fukuoka H, et al. IGF-1 enhances cellular senescence via the reactive oxygen species-p53 pathway. Biochem Biophys Res Commun2012;425:478–84.
12. Holzenberger M, Dupont J, Ducos B, et al. IGF-1 receptor regulates lifespan and resistance to oxidative stress in mice. Nature 2003;421:182–7. [PubMed: 12483226]
13. Kappeler L, De Magalhaes Filho C, Dupont J, et al. Brain IGF-1 receptors control mammalian growth and lifespan through a neuroendocrine mechanism. PLoS Biol 2008;6:e254.
14. Svensson J, Sjogren K, Faldt J, et al. Liver-derived IGF-1 regulates mean life span in mice. PLoS One 2011;6:e22640.

15. Mao K, Quipildor GF, Tabrizian T, et al. Late-life targeting of the IGF-1 receptor improves healthspan and lifespan in female mice. Nat Commun 2018;9:2394. [PubMed: 29921922]
16. Percie du Sert N, Hurst V, Ahluwalia A, et al. The arrive guidelines 2.0: Updated guidelines for reporting animal research. PLoS Biol 2020;18:e3000410.
17. Liu JY, Souroullas GP, Diekman BO, et al. Cells exhibiting strong p16 (INK4a) promoter activation in vivo display features of senescence. Proc Natl Acad Sci U S A 2019;116:2603–2611. [PubMed: 30683717]
18. Hall BM, Balan V, Gleiberman AS, et al. P16(INK4a) and senescence-associated beta-galactosidase can be induced in macrophages as part of a reversible response to physiological stimuli. Aging (Albany NY) 2017;9:1867–1884. [PubMed: 28768895]
19. Chung SI, Horton JA, Ramalingam TR, et al. IL-13 is a therapeutic target in radiation lung injury. Sci Rep 2016;6:39714. [PubMed: 28004808]
20. Groves AM, Johnston CJ, Misra RS, et al. Whole-lung irradiation results in pulmonary macrophage alterations that are subpopulation and strain specific. Radiat Res 2015;184:639–49. [PubMed: 26632857]
21. Groves AM, Johnston CJ, Williams JP, et al. Role of infiltrating monocytes in the development of radiation-induced pulmonary fibrosis. Radiat Res 2018.
22. Ucero AC, Bakiri L, Roediger B, et al. FRA-2-expressing macrophages promote lung fibrosis in mice. J Clin Invest 2019;129:3293–3309. [PubMed: 31135379]
23. Wiley CD, Brumwell AN, Davis SS, et al. Secretion of leukotrienes by senescent lung fibroblasts promotes pulmonary fibrosis.JCI Insight 2019;4.
24. Misharin AV, Morales-Nebreda L, Reyfman PA, et al. Monocyte-derived alveolar macrophages drive lung fibrosis and persist in the lung over the life span. J Exp Med 2017;214:2387–2404. [PubMed: 28694385]
25. Gibbons MA, MacKinnon AC, Ramachandran P, et al. Ly6c hi monocytes direct alternatively activated profibrotic macrophage regulation of lung fibrosis. Am J Respir Crit Care Med 2011;184:569–81. [PubMed: 21680953]
26. Satoh T, Nakagawa K, Sugihara F, et al. Identification of an atypical monocyte and committed progenitor involved in fibrosis. Nature 2017;541:96–101. [PubMed: 28002407]
27. Hall BM, Balan V, Gleiberman AS, et al. Aging of mice is associated with p16(INK4a)- and beta-galactosidase-positive macrophage accumulation that can be induced in young mice by senescent cells. Aging (Albany NY) 2016;8:1294–315. [PubMed: 27391570]
28. Tchkonia T, Zhu Y, van Deursen J, et al. Cellular senescence and the senescent secretory phenotype: Therapeutic opportunities. J Clin Invest 2013;123:966–72. [PubMed: 23454759]
29. Rodier F, Coppe JP, Patil CK, et al. Persistent DNA damage signalling triggers senescence-associated inflammatory cytokine secretion. Nat Cell Biol 2009;11:973–9. [PubMed: 19597488]
30. Coppe JP, Desprez PY, Krtolica A, et al. The senescence-associated secretory phenotype: The dark side of tumor suppression. Annu Rev Pathol 2010;5:99–118. [PubMed: 20078217]
31. Kaviratne M, Hesse M, Leusink M, et al. Il-13 activates a mechanism of tissue fibrosis that is completely tgTGF-beta independent. J Immunol 2004;173:4020–9. [PubMed: 15356151]
32. Lee CG, Homer RJ, Zhu Z, et al. Interleukin-13 induces tissue fibrosis by selectively stimulating and activating transforming growth factor beta(1). J Exp Med 2001;194:809–21. [PubMed: 11560996]
33. Krishnamurthy J, Torrice C, Ramsey MR, et al. INK4a/ARF expression is a biomarker of aging. J Clin Invest 2004;114:1299–307. [PubMed: 15520862]
34. Kurmasheva RT, Houghton PJ. IGF-1 mediated survival pathways in normal and malignant cells. Biochim Biophys Acta 2006;1766:1–22. [PubMed: 16844299]
35. Obradovic M, Zafirovic S, Soskic S, et al. Effects of IGF-1 on the cardiovascular system. Curr Pharm Des 2019;25:3715–3725. [PubMed: 31692426]
36. Davaadelger B, Duan L, Perez RE, et al. Crosstalk between the IGF-1R/Akt/mTORc1 pathway and the tumor suppressors p53 and p27 determines cisplatin sensitivity and limits the effectiveness of an IGF-1R pathway inhibitor. Oncotarget 2016;7:27511–26. [PubMed: 27050276]

37. Chitnis MM, Lodhia KA, Aleksic T, et al. IGF-1R inhibition enhances radiosensitivity and delays double-strand break repair by both non-homologous end-joining and homologous recombination. Oncogene 2014;33:5262–73. [PubMed: 24186206]
38. Yavari K, Taghikhani M, Maragheh MG, et al. siRNA-mediated IGF-1R inhibition sensitizes human colon cancer SW480 cells to radiation. Acta Oncol 2010;49:70–5. [PubMed: 20001499]
39. Allen GW, Saba C, Armstrong EA, et al. Insulin-like growth factor-1 receptor signalling blockade combined with radiation. Cancer Res 2007;67:1155–62. [PubMed: 17283150]
40. Jayanth VR, Belfi CA, Swick AR, et al. Insulin and insulin-like growth factor-1 (IGF-1) inhibit repair of potentially lethal radiation damage and chromosome aberrations and alter DNA repair kinetics in plateau-phase A549 cells. Radiat Res 1995;143:165–74. [PubMed: 7631009]
41. Yosef R, Pilpel N, Tokarsky-Amiel R, et al. Directed elimination of senescent cells by inhibition of bcl-w and bcl-xl. Nat Commun 2016;7:11190. [PubMed: 27048913]
42. Chand HS, Harris JF, Mebratu Y, et al. Intracellular insulin-like growth factor-1 induces bcl-2 expression in airway epithelial cells. J Immunol 2012;188:4581–9. [PubMed: 22461702]
43. Childs BG, Baker DJ, Kirkland JL, et al. Senescence and apoptosis: Dueling or complementary cell fates? EMBO Rep 2014;15:1139–53. [PubMed: 25312810]
44. Hernandez DM, Kang JH, Choudhury M, et al. IPF pathogenesis is dependent upon TGF beta induction of IGF-1. FASEB J 2020;34:5363–5388. [PubMed: 32067272]
45. Aston C, Jagirdar J, Lee TC, et al. Enhanced insulin-like growth factor molecules in idiopathic pulmonary fibrosis. Am J Respir Crit Care Med 1995;151:1597–603. [PubMed: 7537587]
46. Spadaro O, Camell CD, Bosurgi L, et al. IGF1 shapes macrophage activation in response to immunometabolic challenge. Cell Rep 2017;19:225–234. [PubMed: 28402847]
47. Keane MP, Gomperts BN, Weigt S, et al. Il-13 is pivotal in the fibro-obliterative process of bronchiolitis obliterans syndrome. J Immunol 2007;178:511–9. [PubMed: 17182591]
48. Zhu Z, Homer RJ, Wang Z, et al. Pulmonary expression of interleukin-13 causes inflammation, mucus hypersecretion, subepithelial fibrosis, physiologic abnormalities, and eotaxin production. J Clin Invest 1999;103:779–88. [PubMed: 10079098]

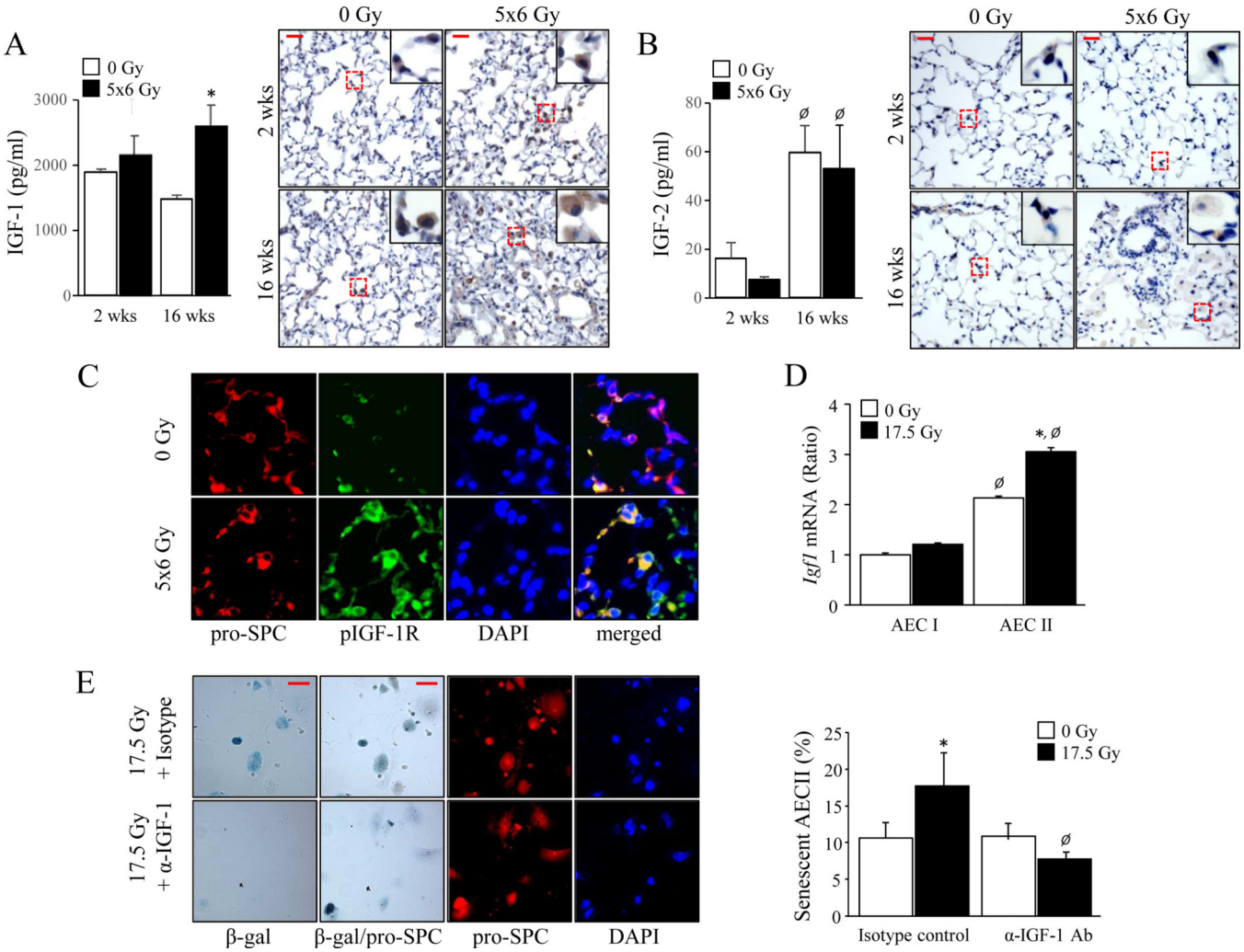

Figure 1. IGF-1 signaling characterizes radiation-induced pulmonary fibrosis.

C57BL6/J mice were exposed to 5 daily fractions of 6 Gy (5×6 Gy) of thoracic irradiation. At 2 and 16 weeks after irradiation, lung (n=5 mice per group) was collected. **A-B)** IGF-1 and IGF-2 expression were examined by ELISA and immunohistochemistry. $p<0.05$ by ANOVA with Tukey's correction: * 0 *vs* 5×6 Gy, Ø 2 *vs* 16 weeks. Scale bars: 30 μm. **C)** Phosphorylation of IGF-1R was evaluated with immunofluorescence in lung collected at 16 weeks after irradiation. AECII were identified by co-labeling with pro-SPC.Scale bar: 15 μm. **D)** A single cell suspension prepared from mouse lungs was irradiated *in vitro* (0 Gy or 17.5 Gy). After a 3-day culture, RNA was isolated from the Aquaporin 5 (AECI) and pro-surfactant-C (AECII) positive populations for quantitative PCR for *IGF-1*. $p<0.05$ by ANOVA with Tukey's correction: * 0 *vs* 17.5 Gy, Ø AECI *vs* AECII. **E)** Senescence associated β-Galactosidase assays were performed in enriched AECII at 3 days after irradiation in the presence of an IGF-1 neutralizing antibody. Scale bars: 15 μm. $p<0.05$ by ANOVA with Tukey's correction: * 0 *vs* 17.5 Gy, Ø Isotype *vs* Anti-IGF-1.Columns: mean, error bars: ± SD.

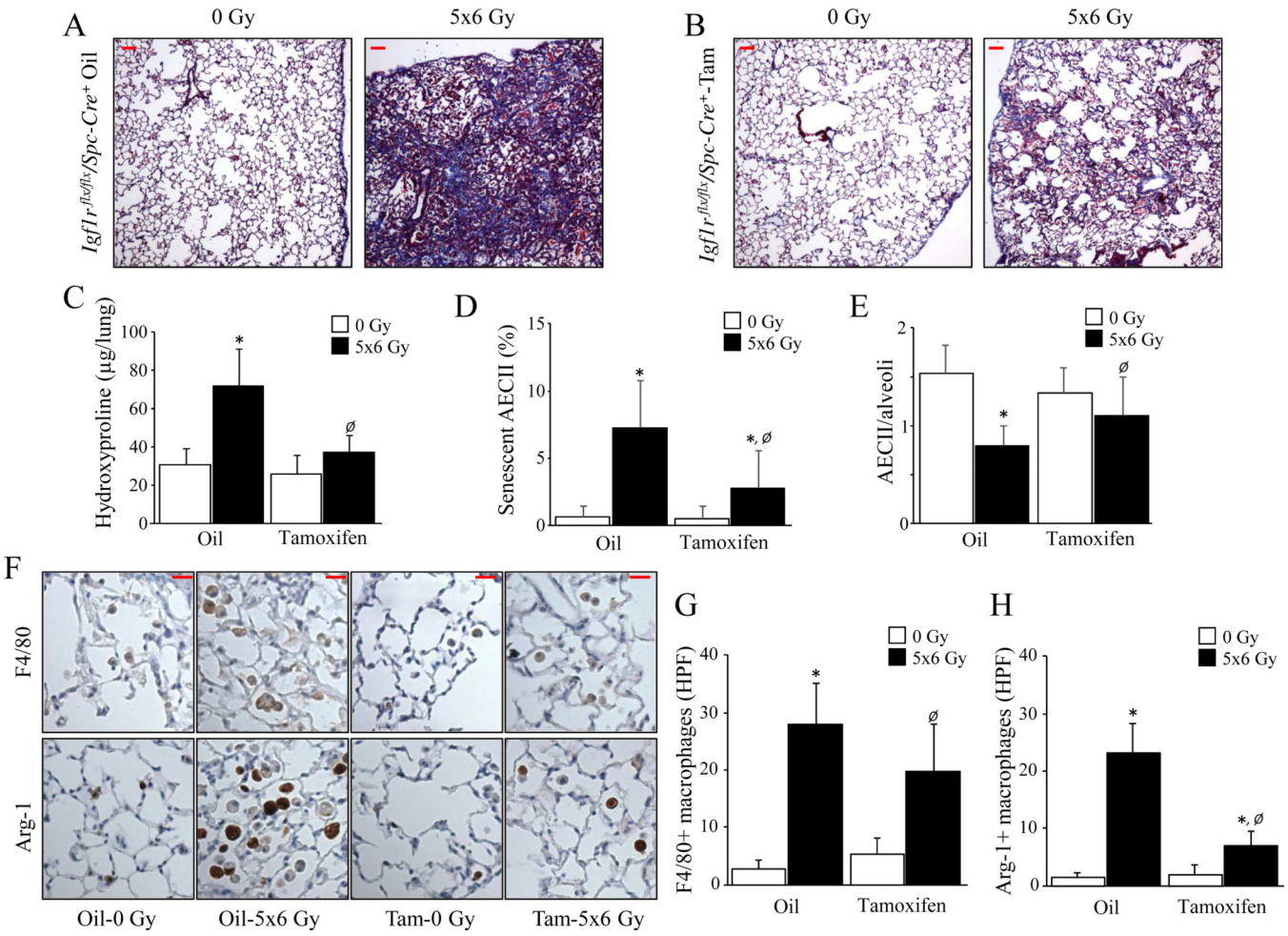

Figure 2. IGF-1R deficiency in AECII protects against radiation-induced lung injury.

Igf1r $^{flx/flx}$/*Spc-Cre*$^{+}$ mice were subjected to 5×6 Gy thoracic irradiation after Oil or Tamoxifen treatment, followed by tissue collection at 16 weeks after irradiation (n≥4). **A-B)** Lung sections collected at 16 weeks after irradiation were subjected to Masson Trichrome staining. Scale bars: 50 µm. **C)** Hydroxyproline content was assessed in lung tissue at 16 weeks after IR. **D)** The percentage of AECII with senescence associated β-Galactosidase activity was assessed in lung tissue. **E)** The number of AECII per alveoli in lung tissue 16 weeks after irradiation was assessed by immunohistochemical assay for pro-Surfactant C. **F-H)** Immunohistochemical assays (brown) with hematoxylin counterstaining (blue) were performed to investigate macrophage accumulation in lungs 16 weeks after irradiation (F4/80: total macrophages, Arginase-1: M2 macrophages). Representative high-power images are presented. Scale bars: 20 µm. * 0 *vs* 17.5 Gy, Ø Oil *vs* Tamoxifen. Columns: mean, error bars: ± SD, each symbol: $p<0.05$; ANOVA with Tukey's correction.

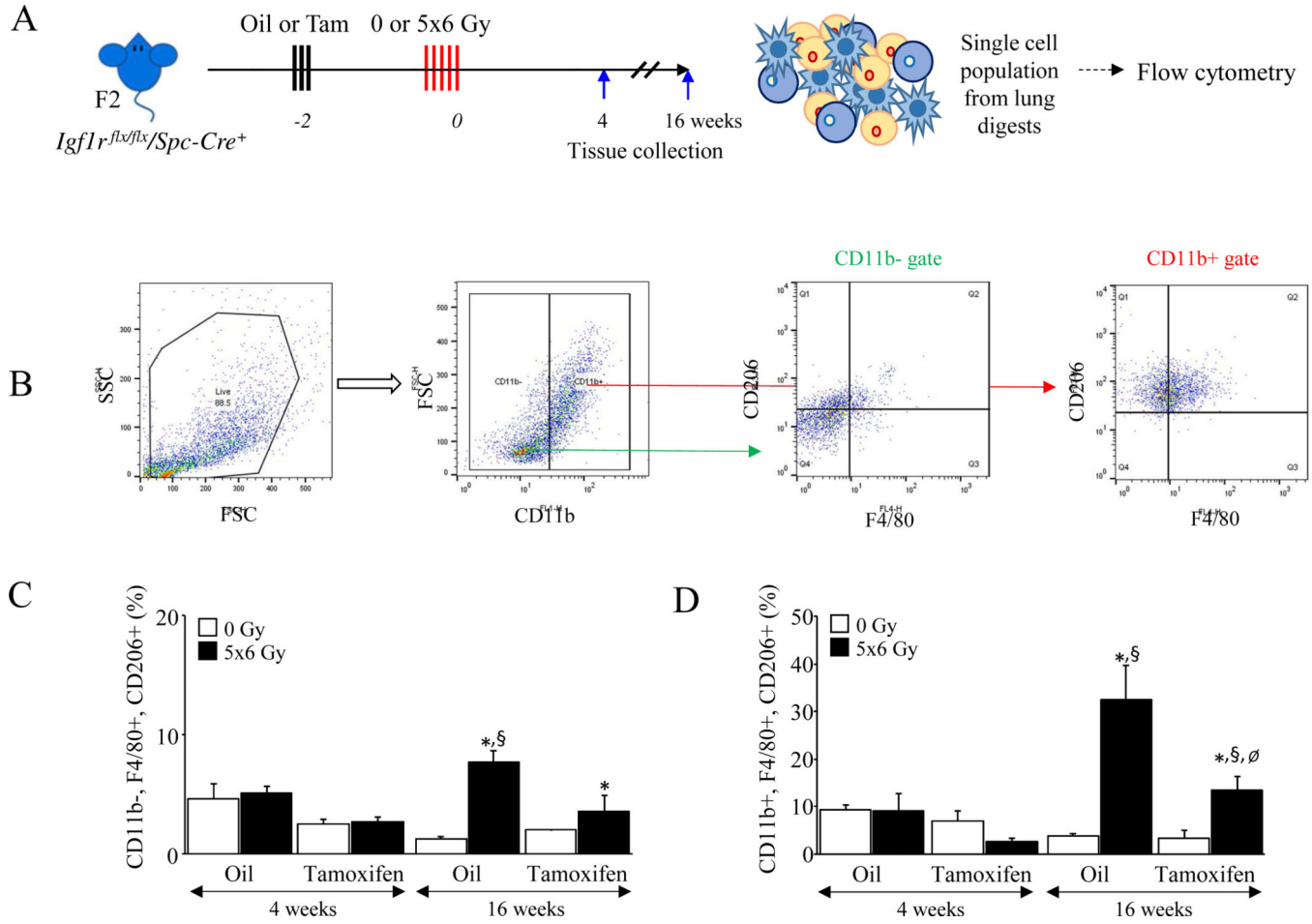

Figure 3. Deficiency of IGF-1R reduces the accumulation of M2 macrophages in irradiated lungs.

A) *Igf1r* $^{flx/flx}$/*Spc-Cre*$^{+}$ mice (n≥4) were subjected to 5×6 Gy thoracic radiation or maintained unirradiated (0 Gy) after Oil or Tamoxifen administration. Single cell suspensions were prepared from each group of lung digests and analyzed via flow cytometry at 16 weeks after irradiation. **B-D)** A sequential gating strategy was developed to examine the percent of CD11b+, F4/80+, CD206+ or CD11b−, F4/80+, CD206+ macrophages in whole lung cell suspensions (left scattergrams). Bar graphs represents the percent of infiltrating (CD11b+, F4/80+, CD206+) or residential (CD11b−, F4/80+, CD206+) M2 macrophages in each group of lungs. * 0 *vs* 5×6 Gy, ^{Ø} Oil *vs* Tamoxifen, § vehicle *vs* ABT263. Columns: mean, error bars: ± SD, each symbol: p<0.05; ANOVA with Tukey's correction.

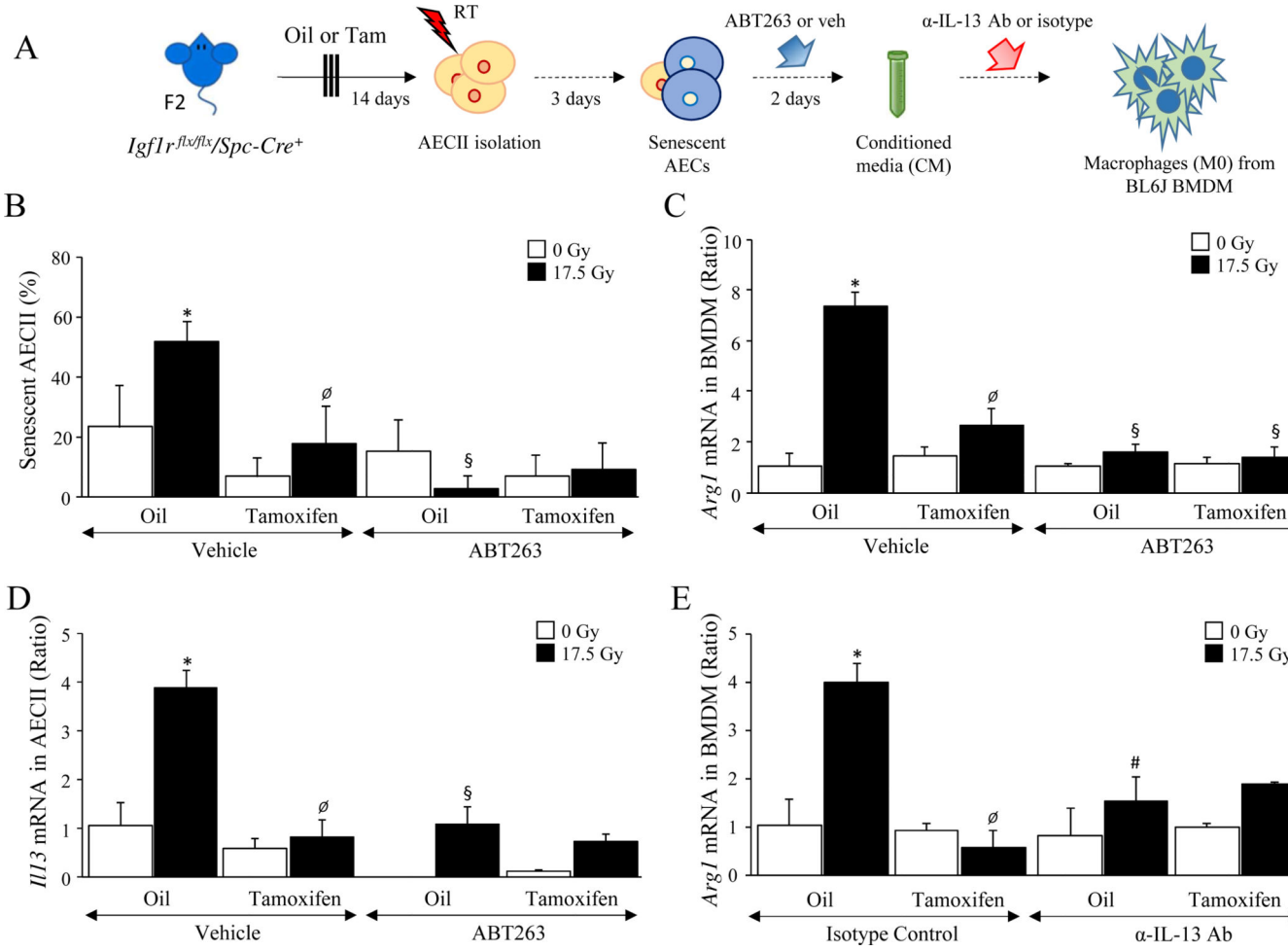

Figure 4. Deficiency of IGF-1R reduces the levels of IL-13 secretion from AECII and results in reduction of M2 type polarization.

A) AECII were enriched from single cell suspensions generated from *Igf1r* $^{flx/flx}$/*Spc-Cre*$^{+}$ mice (n≥4) treated with oil or Tamoxifen. Conditioned media (CM) was generated from primary AECII cultures exposed to irradiation (0 Gy or 17.5 Gy), followed by the treatment of ABT263 or vehicle. Collected CM was applied to BMDM cultures to investigate the effect on macrophage polarization toward the M2 type. **B)** Senescence associated β-Galactosidase activity was assessed in AECII. **C-E)** The levels of Arg-1 mRNA and IL13 were quantified by real-time PCR in polarized BMDM and AECII. * 0 *vs* 5×6 Gy, ^{Ø} Oil *vs* Tamoxifen, § vehicle *vs* ABT263, $^{\#}$ Isotype control *vs* anti-IL-13 antibody. Columns: mean, error bars: ± SD, each symbol: p<0.05; ANOVA with Tukey's correction.

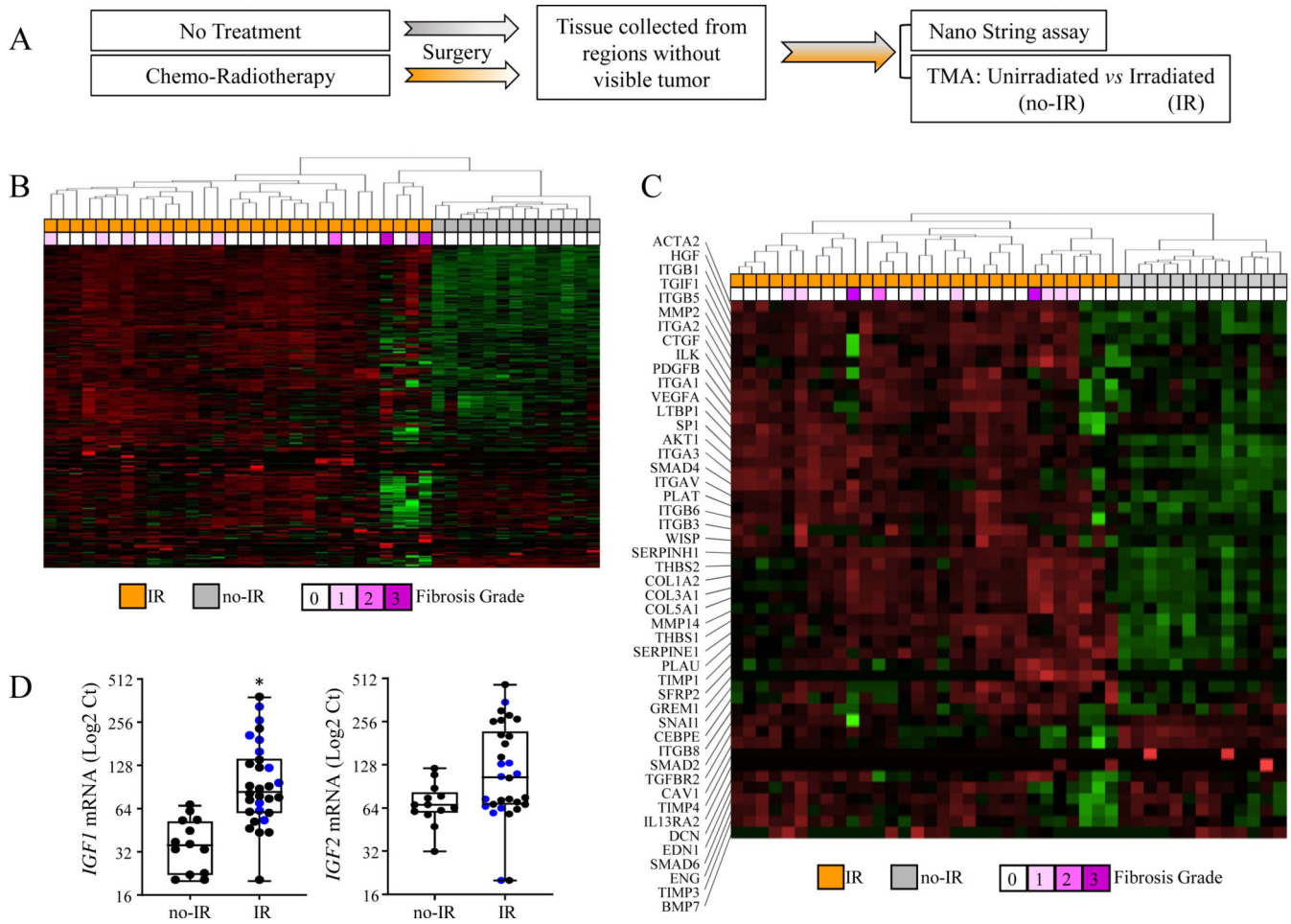

Figure 5. Modification of IGF-1 signaling in lungs from NSCLC patients who received chemo-radiotherapy.

A) To identify pathways associated with senescence, fibrosis, and aging that are altered in irradiated lungs, surgically resected specimens without visible tumor were collected from NSCLC patients treated with chemo-radiotherapy (Irradiated, n=30) or without (Unirradiated, n=13). Total RNA was isolated from each specimen and used to perform NanoString assays. **B)** Gene expression in these tissue samples was evaluated with a custom codeset using the NanoString nCounter Gene Expression Assay. Unsupervised hierarchical clustering was performed. IR: treated with radiotherapy, No-IR: not treated with radiotherapy. Fibrosis: fibrosis scoring (0–3). **C)** The heatmap represents the expression of genes related to fibrosis in lung specimens. **D)** IGF-1 and IGF-2 mRNA levels as assessed by NanoString assay. Blue dots represent fibrotic cores, black dots represent non-fibrotic cores. Boxes: interquartile range, bars in boxes: mean, error bars: Minimum & Maximum, asterisk: $p<0.05$; Mann-Whitney test (non-parametric statistical test).

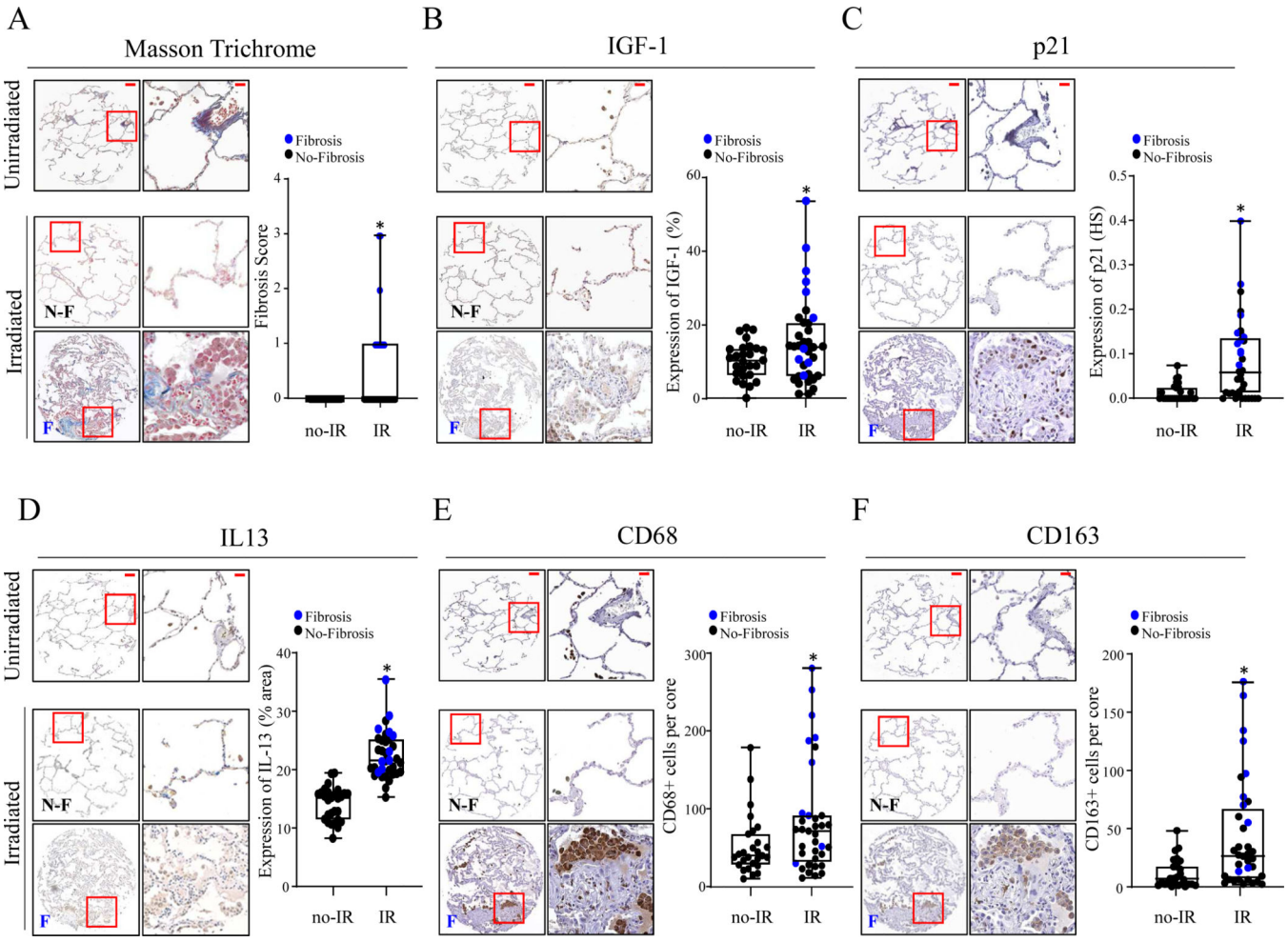

Figure 6. Accumulation of M2 macrophages and induction of p21 protein are increased in fibrotic irradiated lungs.

A) The levels of fibrosis in Masson's-Trichrome stained TMA sections were scored by pathologists. **B-F)** Immunohistochemical assays were performed in TMA sections to evaluate the levels of IGF-1 (% positively stained cells), p21 (histoscore), IL-13 (% of tissue positively stained), and to assess numbers of total macrophages (CD68+) and M2 macrophages (CD163+) (total stained cells per core). Representative immunohistochemical images (left) and bar graphs (right) for matched targets. **N-F**: No-Fibrosis, **F**: Fibrosis. Scale bars: 100 μm in whole core, 20 μm in HPF. Blue dots represent fibrotic cores, black dots represent non-fibrotic cores. Columns: mean, error bars: ± SD, asterisk: $p<0.05$; Mann-Whitney test (non-parametric statistical test).